THE ASTROPHYSICAL JOURNAL, 433:746–756, 1994 October 1

NUMERICAL SIMULATIONS OF MAGNETIC ACCRETION DISKS

JAMES M. STONE
Department of Astronomy, University of Maryland, College Park, MD 20742
AND
MICHAEL L. NORMAN[1]
National Center for Supercomputing Applications, 5600 Beckman Institute, Drawer 25, University of Illinois at Urbana-Champaign, 405 North Mathews Avenue, Urbana, IL 61801
Received 1993 December 14; accepted 1994 March 30

ABSTRACT

The global evolution of magnetic accretion disks is studied by means of time-dependent numerical simulations. Ideal magnetohydrodynamics is used to compute the evolution; the simulations assume the disk is adiabatic, axisymmetric, and initially threaded by a purely axial magnetic field. These restrictions permit a large number of exploratory simulations to be performed. The evolution of both Keplerian and sub-Keplerian disks with a variety of magnetic field strengths is investigated. In the case of an initially sub-Keplerian disk, collapse of the disk is halted at the centrifugal barrier, and rapid wind-up of the magnetic field results in the production of a strongly collimated, magnetic-pressure–driven wind. Although the evolution of the disk in this case is relatively independent of the magnetic field, the detailed properties of the wind are not. Surprisingly, in the case of an initially Keplerian disk, we also find collapse of the disk occurs on orbital timescales regardless of the initial field strength. In the case of an initially strong field the collapse is driven by external torques (magnetic braking), while in the case of an initially weak magnetic field, the collapse is driven by internal torques (the Balbus-Hawley instability). These simulations indicate that magnetized accretion disks and any magnetically driven winds that are associated with them may be intrinsically unsteady.

Subject headings: accretion, accretion disks — MHD

1. INTRODUCTION

While a complete understanding of anomalous angular momentum transport in accretion disks is still an outstanding unsolved problem, a number of recent investigations have focused attention on the role that magnetic fields might play in this process. For example, Balbus & Hawley (1991, hereafter BH; 1992) have identified a powerful local shear instability in weakly magnetized accretion disks which can produce vigorous angular momentum transport associated with complex and turbulent motions in the nonlinear saturated state (Hawley & Balbus 1991, 1992). Through the use of a local analysis, the properties of the nonlinear stage of the instability is under active investigation (Hawley, Gammie, & Balbus 1994). Following Blandford (1989), one can characterize the torques associated with the BH instability as *internal* in that they redistribute angular momentum within the disk itself. On the other hand, magnetic fields can also remove angular momentum from disks via *external* torques, for example via magnetic braking effects (Mouschovias & Paleologou 1980, hereafter MP), or by the action of a magnetocentrifugal wind (Blandford & Payne 1982). In the latter case, a number of authors have studied steady state magnetohydrodynamic (MHD) winds from disks (Königl 1989; Heyvaerts & Norman 1989; Pelletier & Pudritz 1989; Wardle & Königl 1993) and stars (Shu et al. 1988), as well as steady electrodynamic winds from disks (Lovelace, Wang, & Sulkanen 1987).

Of course, it is quite possible that the global structure and evolution of magnetic accretion disks is affected by both internal and external torques. One would like to identify the physical regime in which one mechanism dominates over the other, to investigate the global evolution of disks in which each and/or both are in effect, and to understand how material at the inner edge of the disk flows onto the central object. In general, these problems will require studying solutions of the time-dependent, nonlinear, multidimensional MHD equations for representative models of accretion disks. Given the difficulty of this task, it is quite likely that the tools of numerical simulation will play an important role in this effort.

In this paper, we present time-dependent numerical simulations of the evolution of magnetic accretion disks as a first step in examining the role of global magnetic fields in the accretion process. In order to make the problem tractable, in this study we limit the physical effects included in the simulations (we assume ideal and adiabatic MHD) and consider only two-dimensional axisymmetric systems. We do not attempt to model accretion onto the central star itself, rather we use a simple flow-through inner boundary condition. These restrictions allow us to consider a wider variety of initial conditions for the disk and magnetic field, allowing us to consider regimes where either internal or external torques are expected to dominate. Moreover, we are able to make contact with previous numerical simulations of hydrodynamic (Hawley 1986; Hawley & Smarr 1986) and MHD (Uchida & Shibata 1985, hereafter US; Shibata & Uchida 1986) accretion.

The time-dependent numerical simulations of magnetic accretion disks performed by US are particularly relevant to this work. These authors concentrated primarily on the dynamical evolution of disks initially in sub-Keplerian rotation. Due to the lack of radial force balance in the initial state, collapse of the disk on a free-fall timescale ensued. Under these conditions, US discovered that a hollow, cylidrical jet could be launched from the collapsing disk due to the gradient of the toroidal

[1] Also Department of Astronomy, University of Illinois at Urbana-Champaign.

component of the wound-up magnetic field, a process they termed the "sweeping-magnetic-twist." In this paper, we present results which confirm the conclusions of US for initially sub-Keplerian disks. However, the primary focus of this paper is the dynamical evolution of magnetized Keplerian accretion disks which are initially in radial force balance.

The most important conclusion that can be reached from our simulations is that the evolution of accretion disks threaded by globally axial magnetic fields is *unsteady* regardless of the initial conditions we have studied. In the case of a weak magnetic field, we find that BH instability grows on an orbital timescale, producing vigorous angular momentum transport and radial collapse of the disk at near free-fall velocities for some fraction of the disk. On the other hand, with magnetic fields strong enough to suppress the instability, we find magnetic braking leads to runaway collapse in the innermost portions of the disk. In some cases, dynamical collapse at near free-fall can lead to the production of a wind which, like the underlying accretion disk, is unsteady. These conclusions are summarized in Figure 1, which presents a schematic flow chart of the evolution of magnetic accretion disks observed in our simulations. That magnetic accretion disks may be intrinsically unsteady is supported by observations of FU Orionis events in accreting T Tauri stars (Hartmann & Kenyon 1985). Moreover, the detailed temporal and spatially resolved observations of the best studied MHD system in astrophysics (the solar corona; Low 1990) reveals such unsteady behavior may be ubiquitous in MHD systems.

The organization of this paper is as follows. In § 2 we describe the numerical methods used, and the initial and boundary conditions used to compute the simulations presented here. In § 3 we present our results; in § 4 we discuss how these results might be affected by relaxing some of the assumptions we have made; in § 5 we conclude.

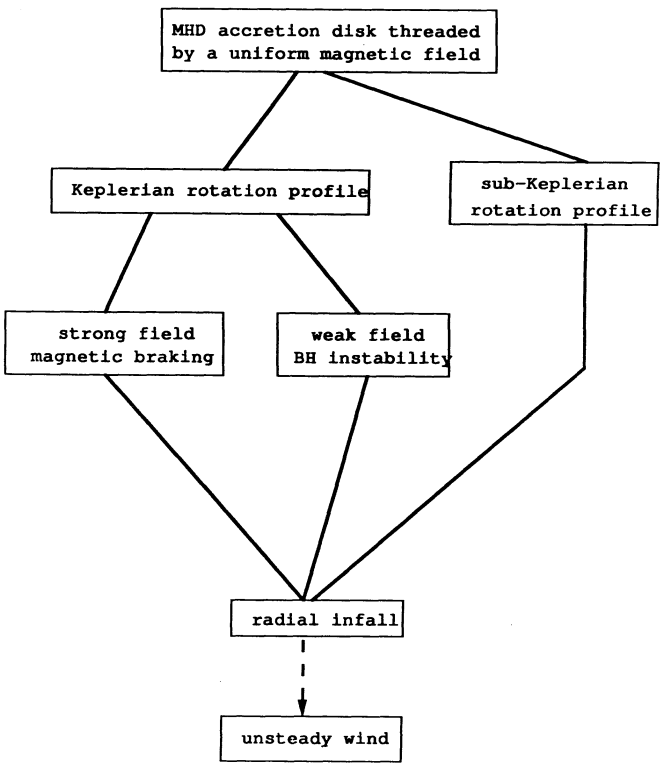

FIG. 1.—Schematic flow chart showing the possible paths of evolution of a magnetic accretion disk as observed in the simulations. Regardless of the initial conditions, all of our simulations lead to radial collapse of the disk.

2. NUMERICAL METHODS

In order to follow the evolution of a magnetic accretion disk we solve the equations of ideal MHD in spherical polar coordinates assuming axisymmetry. We use the ZEUS-2D code described in Stone & Norman (1992a, b) to compute all results presented here. This code has been calibrated using an extensive MHD test suite (Stone et al. 1992a). We assume the gas is adiabatic and is described by a gamma-law equation of state with $\gamma = 5/3$. Although radiative transfer effects could have important consequences for the dynamics of the disk (especially in determining the vertical structure of the disk, or near the inner edge of the disk where a strong radiation field is generated at the boundary layer), we ignore such effects in this first study and concentrate on the MHD evolution alone. By solving the equations of ideal MHD to compute the dynamics, we have assumed that the magnetic flux is "frozen" into the fluid. In more realistic models of magnetic accretion disks, ambipolar diffusion and/or Ohmic diffusivity may allow significant redistribution of magnetic flux in the disk, altering the dynamics of both the disk and any magnetically driven wind which may be present. We discuss in more detail the effect each of these assumptions may have on our results in § 4. Nevertheless, the results presented here provide a useful exploratory study of the evolution of hydromagnetic disks and winds.

To facilitate direct comparison of our results to previous numerical simulations (US), we adopt the same functional form for the density and pressure distributions used by these authors for both the disk and the hot, tenuous corona in which it is embedded. The density and pressure distributions in the disk and corona are

$$\rho(r, \theta) = v \exp\left[\frac{a(L - r)}{r}\right], \tag{1}$$

$$p(r) = \frac{GM\rho_0}{aL} \exp\left[\frac{a(L - r)}{r}\right], \tag{2}$$

where

$$v = \begin{cases} (\xi/\eta)\rho_0 & \text{in the disk } (\pi - \theta_0)/2 \le \theta \le (\pi + \theta_0)/2 , \\ \rho_0 & \text{otherwise} , \end{cases} \tag{3}$$

where M is the mass of the central protostar, a and L are arbitrary, and $\xi/\eta \gg 1$. The disk is chosen to have a constant opening angle θ_0. The self-gravity of the disk is ignored, so that the gravitational potential is determined everywhere by a point mass M located at the origin. The assumed spherical symmetry of the pressure distribution (eq. [2]) implies that we do not model the vertical structure of the disk. Thus, due to the finite thickness of the disk, perfect balance between centrifugal and gravitational forces alone cannot be achieved away from the equatorial plane in the initial state. If the disk is sufficiently thin, the initial vertical settling thus introduced will be small; we find it is completely masked by the subsequent magnetically driven evolution of the disk.

In the interior of the disk, radial pressure gradients are negligible compared to gravitational forces (since $\xi/\eta \gg 1$), and radial force balance is achieved primarily by centrifugal forces.

(Again, we have found initial motions introduced by the lack of perfect radial equilibrium are completely masked by the subsequent dynamical evolution driven by magnetic forces.) The rotational velocity profile of the disk is then

$$v_\phi(r, \theta) = \left(\frac{GM}{\xi r \sin\theta}\right)^{1/2}, \tag{4}$$

where the parameter ξ is introduced to allow for sub-Keplerian initial conditions ($\xi > 1$). The corona is nonrotating, leading to a shear discontinuity at the disk surface. Finally, following US, we choose the initial magnetic field configuration to be purely axial with a uniform strength given by

$$B_0^2 = 4\pi(\delta/\eta) . \tag{5}$$

The initial conditions (eqs. [1]–[5]) are described by three dimensionless parameters: ξ which determines the rotational velocity at a fiducial point $r = L$ in the disk, η which measures the ratio of the square of the sound speed to the square of the rotational velocity at the fiducial point, and δ which measures the square of the Alfvén velocity in the disk to the square of the rotational velocity at the fiducial point. Thus,

$$\xi \equiv \frac{GM}{Lv_\phi^2}, \tag{6}$$

$$\eta \equiv \frac{C_a^2}{\gamma v_\phi^2} = \frac{p}{\rho v_\phi^2}, \tag{7}$$

$$\delta \equiv \frac{v_A^2}{v_\phi^2} = \frac{B_0^2}{4\pi\rho v_\phi^2} . \tag{8}$$

In addition, we are free to choose values for the constants G, M, L, a, θ_0, and ρ_0 used to specify the initial state. We choose the units such that $G = M = L = 1$, and solve the equations on the domain $r \in (0.1, 1.0)$ and $\theta \in (0, \pi/2)$ (equatorial symmetry is assumed). We choose the value for the arbitrary core radius to be $a = 1.0$, the disk opening angle to be $\theta_0 = 0.2$ radians, and the density in the corona to be $\rho_0 = 1.0$ at the fiducial point. With these choices, the more commonly used plasma β parameter is then

$$\beta \equiv \frac{8\pi p}{B^2} = \frac{2\eta}{\delta} \exp\left(\frac{1-r}{r}\right) . \tag{9}$$

An important characteristic of the initial equilibrium state we have defined above is its stability properties. As shown by BH, a magnetic field in a differentially rotating Keplerian accretion disk (in which $d\Omega^2/dR \le -3\Omega^2/R$, where Ω is the orbital frequency and R is a cylindrical radius measured from the rotation axis) is unstable for axisymmetric perturbations of wavenumber k which satisfy

$$kv_A \le \sqrt{3}\Omega , \tag{10}$$

where v_A is the Alfvén speed in the disk. The requirement that the shortest unstable wavelength "fit" inside the disk of thickness H (i.e., $2\pi/k < H$) results in a limit on the field strength implied by

$$\frac{v_A}{H} \le \frac{\sqrt{3}\Omega}{2\pi} . \tag{11}$$

Since the crossing time for an Alfvén wave in the disk is $t_{cr} \sim H/v_A$ and the orbital period is $t_{orb} \sim 2\pi\Omega^{-1}$, equation (11) implies that $t_{cr} \ge t_{orb}/3^{1/2}$ for instability. Using the parameter values chosen above, equation (11) becomes

$$\delta \le \frac{8 \times 10^{-5}}{r} \exp\left(\frac{1-r}{r}\right) . \tag{12}$$

Thus, $\delta < 6$ for instability at $r = 0.1$, while $\delta < 0.003$ for instability at $r = 0.3$.

The fiducial simulation described by US uses dimensionless parameter values of $\xi = 1.6$, $\eta = 2.9 \times 10^{-3}$, and $\delta = 4.7 \times 10^{-3}$. We have computed a large number of cases over a wide range of parameter values which overlap those used by US (Stone 1990). In this paper, we summarize our results by presenting only three simulations computed using values for the parameters of $\xi = 1.0$–1.6, $\eta = 0.01$, and $\delta = 0.1$–0.001 (see Table 1). These choices are motivated primarily by conditions in a protostellar accretion disk, where the particle number density $n = 10^8$ cm^{-3}, $L = 10^{15}$ cm (100 AU), $M = 1$ $M_\odot$, $T = 16$ K, and $B = 0.5$–1.6 mG. We emphasize, however, that our results will be applicable to any combination of physical values which lead to the given values of the dimensionless parameters.

Figure 2 summarizes the problem geometry of the numerical simulations. Typically, we use 80 logarithmically spaced zones in both the radial and polar angular directions with the maximum resolution at the midplane of the disk (so that there

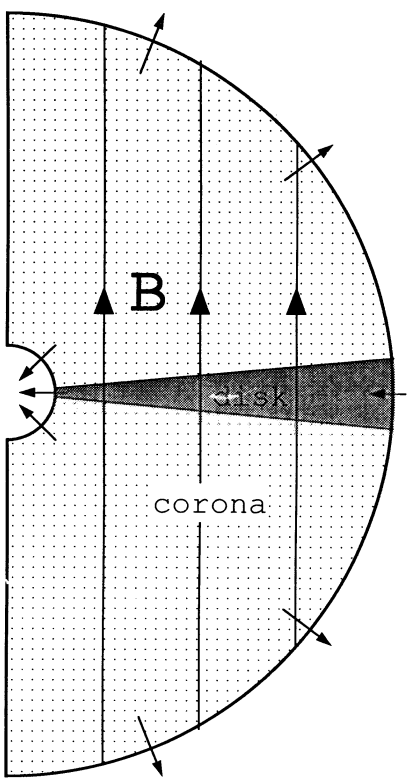

FIG. 2.—Setup of the numerical simulations. The accretion disk, denoted by the shaded region, has a constant opening angle and is threaded by an axial magnetic field. The inner boundary is free-flow (the surface of the accreting object is not modeled). The region above the surface of the disk is filled with hot, tenuous, nonrotating coronal gas in hydrostatic equilibrium.

TABLE 1

PARAMETERS FOR NUMERICAL SIMULATIONS

Run	ξ	η	δ	$\beta(r = 1)$
A	1.6	0.01	0.01	2
B	1.0	0.01	0.1	0.2
C	1.0	0.01	0.001	20

are about 16 zones across the full thickness of the disk) and at the inner radial edge. We assume both axisymmetry and equatorial symmetry and, therefore, compute in only one quadrant. Outflow (free) boundary conditions are used at the inner and outer radii, except where the disk touches the outer boundary $[(\pi - \theta_0)/2 \leq \theta \leq (\pi + \theta_0)/2]$ at which inflow at a rate determined by the solution in the last radial grid point is allowed. Our implementation of outflow boundary conditions implies all outgoing wave and entropy characteristics will be transmitted with only a very small fraction of the incident wave energy reflected. By varying the size of the computational domain, we have checked the reflected wave energy has no measurable effect on the evolution described in this paper (Stone 1990).

3. RESULTS

3.1. *A Sub-Keplerian Disk*

As a first application we attempt to reproduce previous global simulations of magnetic accretion disks (US) by studying the evolution of a sub-Keplerian disk threaded by a uniform axial field. The complete set of parameter values used for this simulation, hereafter referred to as Run A, are given in Table 1. In Figure 3 we plot contours of the density, velocity vectors, and representative poloidal magnetic field lines at 1, 2.5, and 5 orbits of the inner edge of the disk ($r = 0.1$). It is evident from Figure 3 that the disk undergoes dramatic evolution. Radial contraction of the disk produces a pinching of the field lines in the equatorial plane. Outflow above and below the disk is generated after only a few orbits; at orbit 2.5 the outflow is expanding, while by orbit 5 the entire computational domain is filled with outflowing gas. The region near the axis of symmetry contains little or no disk material in either case. This is

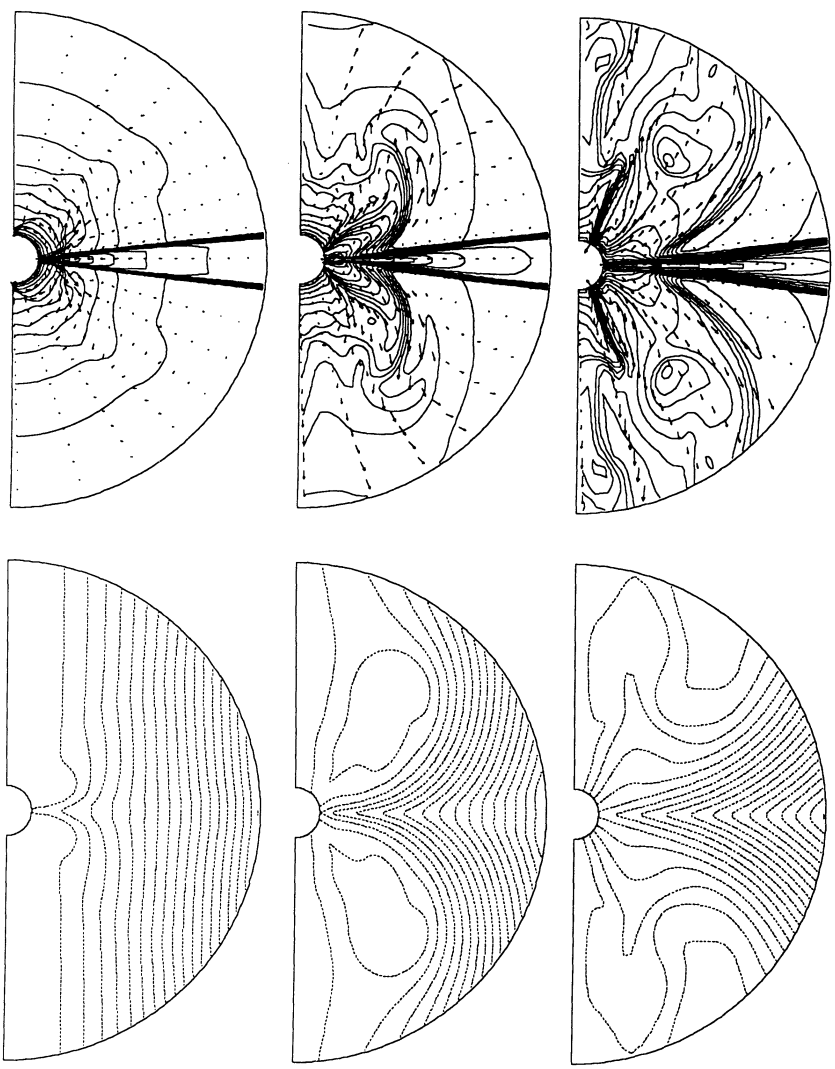

FIG. 3.—Results for sub-Keplerian initial conditions and a weak magnetic field ($\delta = 0.01$) at $t = 1$, 2.5, and 5 orbits of the inner edge of the disk located at $r = 0.1$. *Top*, Contours of the logarithm of the density (*solid lines*) and velocity vectors; *bottom*, representative poloidal magnetic field lines.

likely due to the fact that the field lines in this area enter the inner (free) boundary before piercing the disk; it is therefore not possible to load these field lines with material from the disk. The toroidal component of the magnetic field, plotted in Figure 4, shows a steady and strong gradient along the outflow direction. The growth of this component of the field is very large, $B_\phi \sim 10(B_r^2 + B_\theta^2)^{1/2}$ near the inner boundary, and $\beta_\phi \equiv 8\pi\rho/B_\phi^2 \sim 0.1$ there. It is evident from these figures that our simulations reproduce the result first described by US, that sub-Keplerian disks form strong outflows.

In Figure 5 we quantify the strength of the observed outflow for Run A by plotting the mass flux and kinetic luminosity through each boundary of the computational domain. These fluxes are defined as

$$\mathscr{F}_M(R_b) = 4\pi \int_0^{\pi/2} \rho(R_b, \theta) v_r(R_b, \theta) R_b^2 \sin\theta \, d\theta \,, \qquad (13)$$

$$\mathscr{F}_{KE}(R_b) = 4\pi \int_0^{\pi/2} \tfrac{1}{2}\rho(R_b, \theta)[v(R_b, \theta)]^2 v_r(R_b, \theta) R_b^2 \sin\theta \, d\theta \,, \qquad (14)$$

where R_b is the radius of the boundary at which the flux is computed. There are three curves plotted for each figure. The solid line denotes the fluxes across the inner radial boundary, i.e., the accretion rate (it is always negative). The short-dashed line denotes the fluxes across the outer radial boundary in the domain $(\pi - \theta_0)/2 \le \theta \le (\pi + \theta_0)/2$, i.e., the solid angle subtended by the disk. This is the accretion flux in the disk at the outer boundary (it is always negative). Finally, the long-dashed line denotes the fluxes across the rest of the outer radial boundary. We find that this flux is always positive, thus we label it the outflow rate. The outflow observed in Run A is quite significant. At late times, the flux of mass and energy in the outflow is comparable to the rate at which material flows into the disk at the outer edge and is larger than the accretion rate through the inner boundary. When given in cgs units (and assuming values for the free parameters appropriate to a protostellar disk as given in § 2), then the typical mass and energy flux rates are 10^{-4}–10^{-5} $M_\odot$ yr^{-1} and 0.1 $L_\odot$, which are comparable to those observed for bipolar outflows (Lada 1985). However, in both cases, we have not yet reached a steady state, nor is this possible using the assumption of ideal MHD. This is because magnetic field diffusion, the field strength at the inner edge of the disk will continue to grow and will ultimately prevent further contraction.

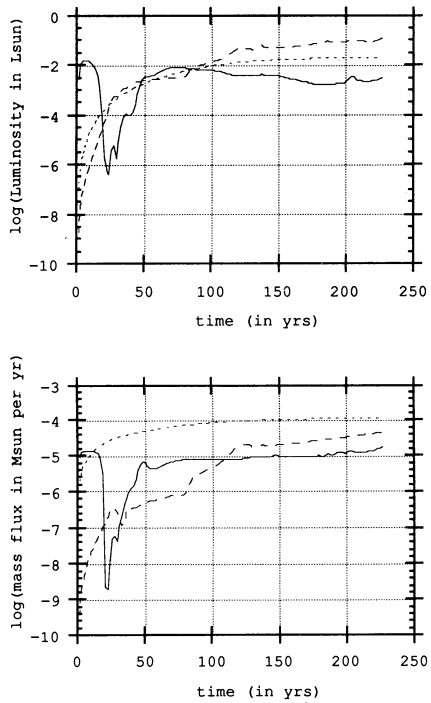

FIG. 5.—Mass fluxes (*top*) and kinetic luminosity (*bottom*) associated with the flow through each boundary for the weak magnetic field and sub-Keplerian initial conditions (Fig. 3). The solid lines denote the inflow across the lower boundary (accretion), the short-dashed line denotes inflow through the outer boundary within the accretion disk, and the long-dashed line denotes the wind. The solutions are scaled to a protostellar disk with fiducial values given in the text. The orbital period at the inner edge of the disk is 10 yr.

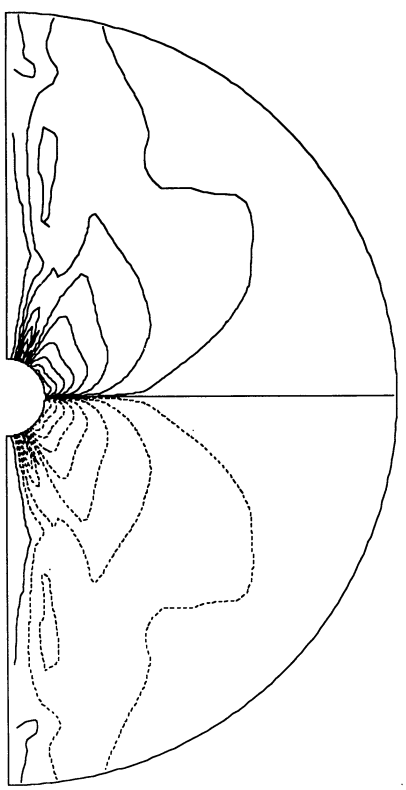

FIG. 4.—Contours of the toroidal magnetic field at $t = 5$ orbits for the disk evolution shown in Fig. 3. Dashed lines denote negative values.

Although not shown here, we have performed a number of sub-Keplerian disk calculations using a variety of magnetic field strengths and topologies (including the "split-monopole" field suggested by Sakurai 1987), and with a variety of numerical resolutions and sizes for the computational domain (Stone 1990). We find that the initial collapse of the disk proceeds in a manner which is largely independent of the assumed field strength or topology. The resulting outflow produced by the collapse is strongly dependent on the magnetic field, however. Stronger fields produce stronger, more highly collimated outflows. The topology of the initial field (i.e., purely axial or diverging) can also affect the degree of collimation. When a computational domain which spans $r \in (0.1, 10)$ is used, we find the outflow becomes collimated into a purely axial jet at

large distances (see, e.g., Norman, Clarke, & Stone 1991, Fig. 3). These results are all consistent with those reported by US.

A fundamental question arising from these simulations is how to identify the force responsible for driving the mass outflow. In order to test the possibility that the outflow is a Blandford & Payne centrifugal-driven wind, we have plotted the Alfvén surface in these simulations and attempted to apply the Michel (1969) scaling law (i.e., $v_{r,\mathrm{A}} \propto \Omega R_{\mathrm{A}}$, where $v_{r,\mathrm{A}}$ is the radial velocity along a particular field line at the Alfvén point located at R_{A} and Ω is the angular velocity of the underlying disk at the point where that field line intercepts the disk). This procedure is complicated by the fact that the Alfvén surface in these dynamical outflows is nonsteady. Nonetheless, we find that in all simulations; the Michel scaling does not apply anywhere along the Alfvén surface. This suggests that the wind is not generated by magnetocentrifugal forces. US attribute the outflow to the gradient of the toroidal magnetic field pressure, i.e., $\nabla B_\phi^2/8\pi$. While we agree with this conclusion, we emphasize here that the emergence of this strong gradient requires the dynamical collapse of the disk.

One way to isolate the effect of the magnetic field on the dynamical evolution is to compare our results with purely hydrodynamical studies of accretion. Hawley (1986) has performed time-dependent numerical simulations of hydrodynamical accretion flows onto black holes. His results demonstrated that the accretion of material with nonzero angular momentum produces a centrifugal barrier at some radius below which the rotational velocity diverges. For material initially in orbit at radius R with velocity $v_\phi = (\xi r)^{-1/2}$, the centrifugal barrier occurs at $r = (R/\xi)$ provided that angular momentum is conserved.

In the case of MHD accretion, however, magnetic braking effects may remove angular momentum from the collapsing disk. Following MP, the magnetic braking timescale can be defined as the time it takes torsional Alfvén waves propagating into the external medium to traverse an amount of material whose moment of inertia is the same as the moment of inertia of the disk. For an aligned rotator, as we have set up here, this timescale is

$$t_{\parallel} = \sqrt{\frac{\rho_d}{\rho_x}}\frac{H}{v_{\mathrm{A}}} = \frac{\xi r \theta_0}{2\sqrt{\delta\eta}} \exp\left[\frac{(1-r)}{2r}\right], \qquad (15)$$

where ρ_d and ρ_x are the densities in the disk and the external medium, respectively, and H is the disk half-thickness. For the parameters of Run A, the magnetic braking timescale at small radii is much larger than the orbital timescale ($t_{\mathrm{orb}} = 2\pi r/v_\phi = 2\pi r^{3/2}$); i.e., $t_{\parallel} \ll t_{\mathrm{orb}}$. Thus, magnetic braking should not be important in the initial evolution of the disk.

We conclude, therefore, that the evolution of an initially sub-Keplerian disk proceeds at first much like the hydrodynamical accretion studies by Hawley. For the case $\xi = 1.6$ on the domain $r \in (0.1, 1.0)$ all material which is initially at radii greater than $r = 0.16$ will encounter a centrifugal barrier on the grid. For $r > 0.16$, material will collapse on an orbital timescale, hit the centrifugal barrier, shock, and stagnate. In the hydrodynamical simulations of Hawley (1986), the hot shocked gas forms a bubble which flows slowly back along the surface of the disk but does not produce a strongly collimated outflow. Using a nonmagnetic disk ($\delta = 0$) which is otherwise identical to Run A, we have confirmed this result within the context of the present simulations (Stone 1990). The outflow observed in Run A and in the simulations of US must therefore be driven by magnetic forces. Detailed analysis of the axial component of the forces on the fluid near the centrifugal barrier indeed reveals the axial gradient of the toroidal magnetic pressure is dominant.

The axial outflow observed in the MHD simulations is therefore a result of *both* the strong gradient in the toroidal magnetic field and the assumed initial conditions (which lead to an essentially hydrodynamical collapse of the disk on an orbital timescale). The infalling gas hits the centrifugal barrier, shocks, and stagnates. The hot, rapidly rotating, magnetic gas then winds up the field lines very tightly, generating a strong gradient in magnetic pressure which forces the fluid poleward. At higher latitudes, the axial field completes the collimation of the outflow into an axial jet. However, we do not consider such a strongly sub-Keplerian rotation profile to be a useful model for an accretion disk, thus the relevance of this scenario to the MHD winds responsible, e.g., for bipolar outflows is quenstionable.

3.2. *A Keplerian Disk with a Strong Field*

A Keplerian rotation profile is a more realistic initial condition for the disk. Therefore, the second simulation we describe, hereafter referred to as Run B, starts with a Keplerian rotation profile ($\xi = 1$) and a strong magnetic field ($\delta = 0.1$; see Table 1). To illustrate the radial evolution of the disk more clearly, the disk is truncated at $r = 0.3$, so that the inner edge of the disk is removed from the inner boundary. From equation (12) we find this disk should be stable to the BH instability at all radii. Figure 6 plots contours of the density, velocity vectors, and representative magnetic field lines at times of 0.2, 1, and 2 orbits of the inner edge of the disk ($r = 0.3$). Once again we find the disk undergoes dramatic evolution in only two orbits. The inner edge of the disk collapses from $r = 0.3$ to $r = 0.1$ (the inner boundary) in this time, dragging magnetic field lines with it, producing a characteristic pinching in the equatorial plane. At larger radii, the disk is fattened, primarily by toroidal magnetic pressure gradients. Since this disk is BH stable, we conclude the evolution of the disk is driven by magnetic braking effects, in other words by external torques. From equation (15), the magnetic braking timescale for Run B is $t_{\parallel} \approx 3$ orbits at all radii in the initial state. Although this timescale will vary substantially as the disk evolves, it is consistent with the observed evolution in Figure 6. In fact, high time resolution animations of the evolution of the disk clearly show a pattern of internal Alfvén wavefronts in the disk, with partial reflections and transmissions occurring at the disk surface, in a manner expected for a magnetically braked aligned rotator (MP; Stone et al. 1992a).

In Figure 7, we plot contours of the toroidal component of the magnetic field at $t = 2$ orbits for the central regions of the grid ($r < 0.5$) only. This component shows a smooth decline in strength away from the equatorial plane. In Figure 8 we plot the flux of angular momentum *carried by the fluid*, defined as

$$\mathscr{F}_L = \rho r v_\phi \boldsymbol{v}\,, \qquad (16)$$

as vectors at $t = 2$ orbits for $r < 0.5$. Within the disk, the flux is everywhere negative, indicating accretion, with the largest values occurring at the midplane. Above the disk, there are extended regions of very low amplitude positive flux. This pattern reflects the action of an external torque; angular momentum is lost from the disk and deposited in the corona, driving accretion and outflow, respectively.

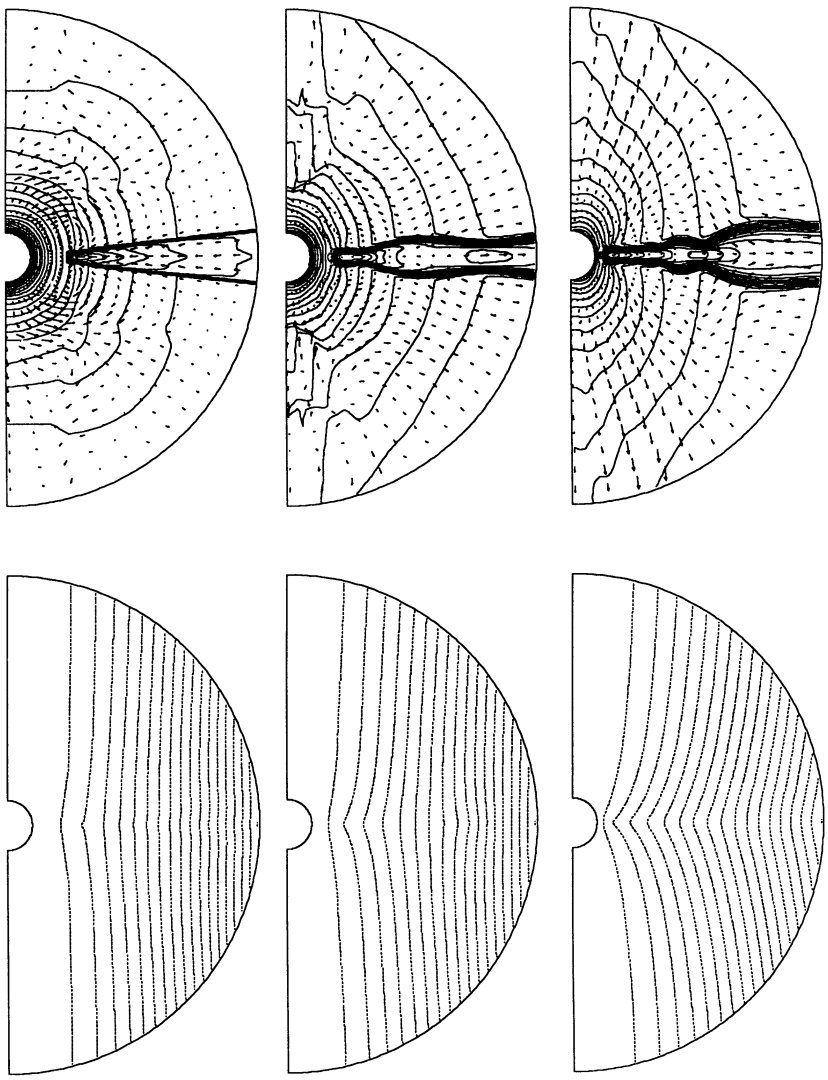

FIG. 6.—Results for Keplerian initial conditions and a strong magnetic field ($\delta = 0.1$) at $t = 0.2$, 1, and 2 orbits of the inner edge of the disk located at $r = 0.3$. *Top*, Contours of the logarithm of the density (*solid lines*) and velocity vectors; *bottom*, representative poloidal magnetic field lines.

Run B demonstrates that a magnetically braked disk undergoes rapid radial collapse. However, this rapid evolution is driven in part by the small magnetic braking timescale in comparison to an orbital time. The magnetic braking timescale can be increased by increasing the ratio of the density in the disk to the corona; in Run B this ratio is 100. (Note that increasing $t_{\|}$ by increasing H or decreasing v_A leads to completely different effects caused by magnetic instabilities; see next section). In order to investigate the evolution of disks with longer magnetic braking timescales, we have considered models in which the disk-to-corona density ratio is as large as 10^3. We find, however, that such large density contrasts are not preserved during the subsequent evolution; settling introduced by the lack of strict vertical equilibrium and axial motions produced by Alfvén waves result in mass diffusion at the surface of the disk. Material in these surface layers, with a density intermediate between that of the disk and corona, is then strongly braking and begins to collapse radially. The subsequent evolution then becomes complex as the magnetic field is sheared first radially, and then toroidally. Once again, however, we find the net result is that some fraction of the disk undergoes rapid radial collapse. Since any realistic model of a dense accretion disk will include vertical stratification, radial collapse of at least the lower density surface layers may be unavoidable for a disk dominated by magnetic braking.

3.3. *A Keplerian Disk with a Weak Field*

To investigate the global evolution of a magnetic accretion disk which is initially BH unstable, we have repeated Run B with a weaker initial field strength ($\delta = 0.001$; see Table 1). The resulting evolution for this calculation, hereafter referred to as Run C, is shown in Figure 9, which plots contours of the density, velocity vectors, and representative poloidal magnetic field lines at $t = 0.2$, 1, and 2 orbits of the inner edge of the disk ($r = 0.3$). Once again, the disk collapses dynamically on an orbital timescale. Perhaps most interesting is the pattern of magnetic field lines, which unlike Figure 6 does not show simple radial pinching. In fact, the radial component of the field can be seen to undergo reversals in direction in both the corona and the disk, resulting in a pattern of radially aligned

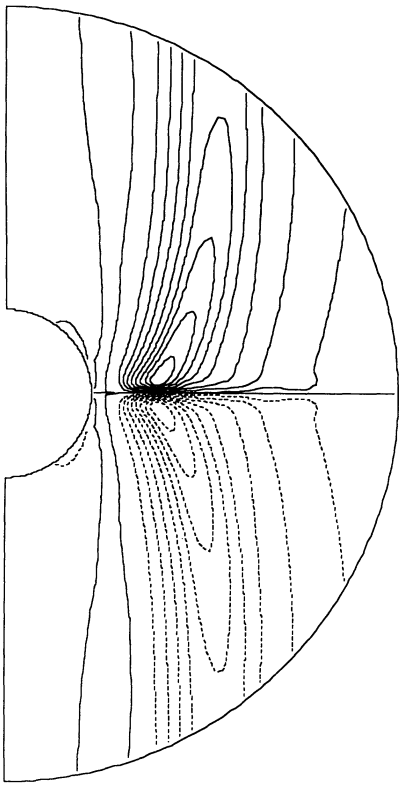

FIG. 7.—Contours of the toroidal magnetic field at $t = 2$ orbits for the disk evolution shown in Fig. 6. Only the inner portion of the computational grid ($r < 0.5$) is shown. Dashed lines denote negative values.

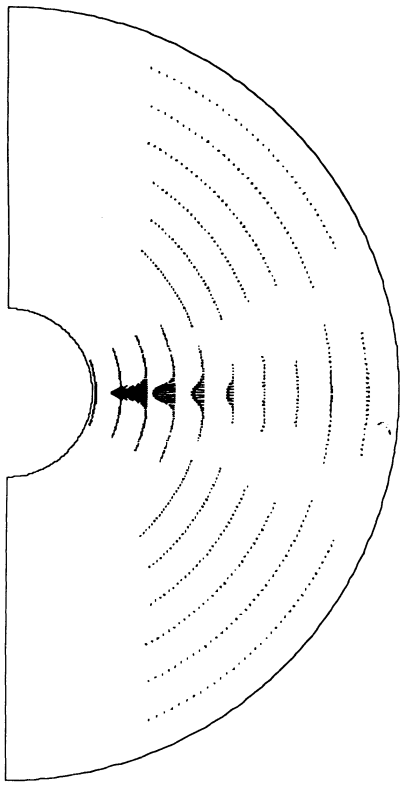

FIG. 8.—Vectors of the angular momentum flux at $t = 2$ orbits for the disk evolution shown in Fig. 6. Only the inner portion of the computational grid ($r < 0.5$) is shown.

kinks in the field lines. Time-dependent simulations of the nonlinear stage of the axisymmetric BH instability (Hawley & Balbus 1992) have demonstrated that vertical magnetic fields produce a radially streaming solution in the saturated state composed of alternate layers of fluid moving in opposite directions. These channels evolve to the largest length scale available on the grid within a few orbits. This surprising result has many of the properties of an exact nonlinear channel solution for an initially vertical magnetic field found by Goodman & Xu (1993).

The pattern of magnetic field lines seen in Run C after a few orbits (Fig. 9) is strikingly similar to that expected for a fully developed streaming solution. The channels occupy the largest available length scale (the thickness of the disk), giving an outward-streaming channel at the midplane of the disk surrounded by inward-moving channels at each surface. This suggests, therefore, that the evolution and radial collapse of the disk is driven by the nonlinear growth of axisymmetric modes of the BH instability (which can start either from linear perturbations produced at the shear discontinuity at the disk surface, or by motions caused by the lack of strict equilibrium in the initial state).

In Figure 10, we plot contours of the toroidal component of the magnetic field at $t = 2$ orbits for the inner regions of the disk ($r < 0.5$) only. Now the field does not show a smooth decrease away from the equatorial plane, rather several reversals in sign are evident within the disk. Each sign reversal in B_ϕ corresponds to a sign reversal in B_r. The large gradients in the toroidal magnetic pressure result in a fattening of the disk evident at late times.

In Figure 11 we plot both the angular momentum flux $\mathscr{F}_L$ defined by equation (16) and the difference in the local value of the angular momentum compared to Keplerian rotation,

$$\Delta L = \rho(rv_\phi - \sqrt{GMr}) \,. \tag{17}$$

We find the largest fluxes of angular momentum are confined to the disk, consistent with the action of an internal torque. Moreover, we find the flux is positive (i.e., outward) in the midplane, but negative (i.e., inward) at the surfaces of the disk. Thus the radially streaming channel solutions are clearly evident. The contours of ΔL defined by equation (17) clearly indicate that the outward-directed stream at the midplane consists of fluid with an excess of angular momentum compared to Keplerian rotation, whereas the inward-directed streams at the surface are composed of fluid with a deficit of angular momentum compared to Keplerian rotation. In Figure 12 we plot the time evolution of the toroidal magnetic energy [i.e., $\int_V (B_\phi^2/8\pi)dV$] in the disk in units of the initial magnetic energy in the disk for both Runs B and C. In Run B (BH stable), plotted as a solid line, we find the magnetic energy oscillates around a small mean value; it shows no sign of sustained growth. The crossing time for an Alfvén wave in the disk is $t_{cr} \sim H/v_A \sim 0.3$ orbits, which is close to the observed timescale for the oscillations of about 0.1 orbits. On the other hand, the toroidal magnetic energy in the disk for Run C (BH unstable), plotted as a dashed line, remains small for the first 0.5 orbits, but then shows strong and sustained growth thereafter. Beyond orbit 1, the toroidal energy in Run C exceeds that in Run B by more than two orders of magnitude. This rapid

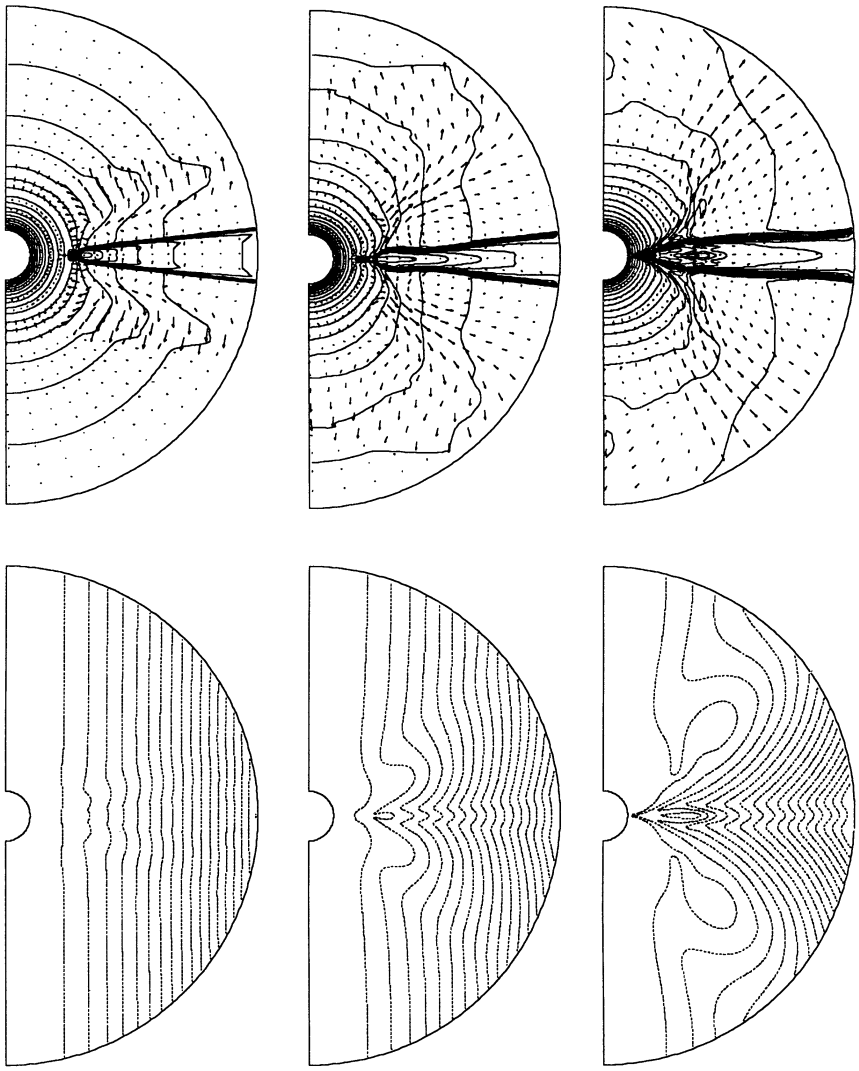

FIG. 9.—Results for Keplerian initial conditions and a weak magnetic field ($\delta = 0.001$) at $t = 0.2$, 1, and 2 orbits of the inner edge of the disk located at $r = 0.3$. *Top*, Contours of the logarithm of the density (*solid lines*) and velocity vectors; *bottom*, representative poloidal magnetic field lines.

growth is consistent with amplification via the BH instability. In fact, Figures 10–12 all strongly support the conclusion that the evolution of the disk in Run C is driven by the nonlinear stage of an axisymmetric mode of the BH instability.

4. THE EFFECTS OF ADDITIONAL PHYSICS

4.1. *Nonideal MHD*

As discussed in Stone & Norman (1992b) and Stone et al. (1992a), the form of the induction equation solved in ZEUS-2D assumes ideal MHD; i.e., it can only account for the effect of the advection term in the generalized Ohm's Law. Thus, in this work, we ignore the effects of Ohmic resistivity, the Hall current, and ambipolar diffusion. Since the Hall current will be negligible unless the electron-ion drift velocity is large, a situation not expected in accretion disks (Königl 1989), in this section we confine our discussion to the potential effects of Ohmic resistivity and ambipolar diffusion to our results.

In most atrophysical systems, Ohmic diffusivity is negligible unless the diffusion coefficient is anomalously large in comparison with classical microphysical transport processes. For example, turbulent reconnection is often invoked as one mechanism for achieving a large effective diffusivity. Limiting the growth of the toroidal component of the field with diffusion may reduce the magnitude of the outflow driven by magnetic pressure gradients observed in our sub-Keplerian simulations (Run A). A large resitivity will also affect the propagation of nonlinear Alfvén waves, which can potentially modify the magnetic braking of the disk (Run B). We point out, however, that since both Runs A and B are stable (especially with respect to the BH instability), simply assuming they are affected by a large turbulent resistivity may not be self-consistent. Thus, although it may be possible to model these processes numerically by assuming an anomalously large Ohmic diffusivity a priori, we have not done so here. Turbulent reconnection may provide a saturation mechanism for the nonlinear stage of the BH instability; however, self-consistent modeling of this process will require high-resolution, three-dimensional simulations. We point out that our simulations will contain a large effective resistivity and reconnection rate associated with numerical diffusion. However, the truncation errors responsible for the numerical diffusion of the magnetic field do

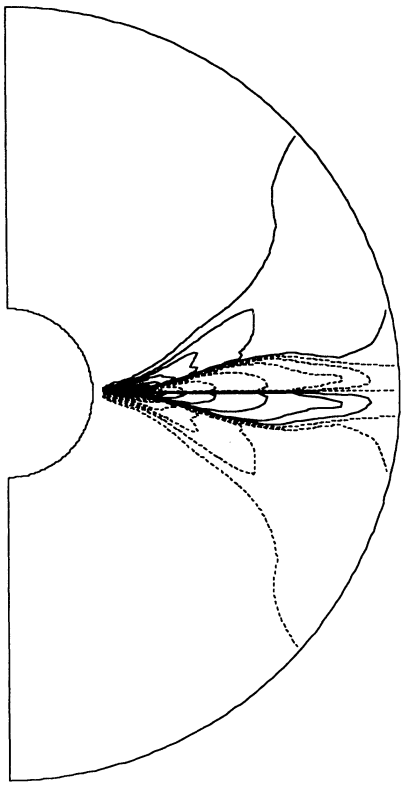

FIG. 10.—Contours of the toroidal magnetic field *at* $t = 2$ orbits for the disk evolution shown in Fig. 9. Only the inner portion of the computational grid ($r < 0.5$) is shown. Dashed lines denote negative values.

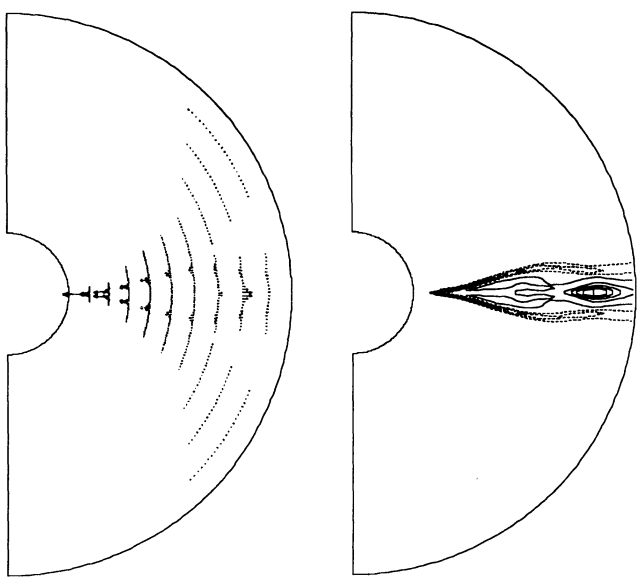

FIG. 11.—Vectors of the angular momentum flux (*left*) and contours of the difference of the local value of angular momentum from Keplerian rotation (*right*) at $t = 2$ orbits for the disk evolution shown in Fig. 9. Only the inner portion of the computational grid ($r < 0.5$) is shown. Dashed lines denote negative values.

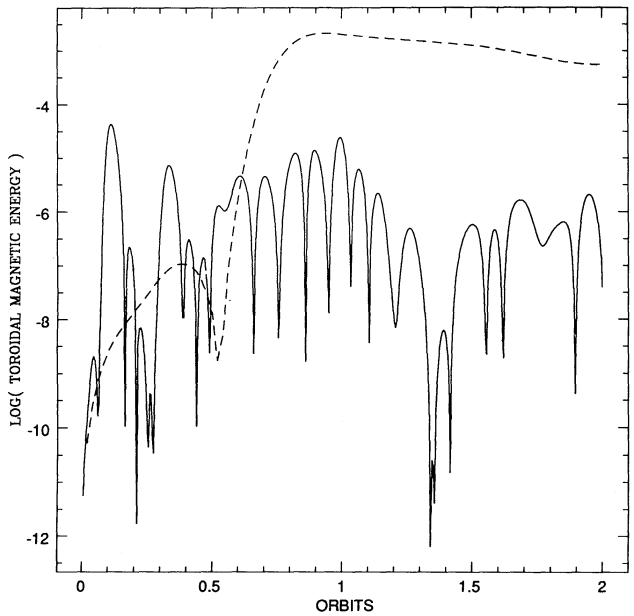

FIG. 12.—Evolution of the toroidal magnetic energy in the disk for Run B (*solid line*) and Run C (*dashed line*) plotted in units of the initial total magnetic energy in the disk. In Run B, the toroidal magnetic energy oscillates around a small mean value, consistent with field generation via shear Alfvén waves. In Run C, the toroidal magnetic energy shows strong sustained growth after 0.5 orbits, consistent with the action of the BH instability.

not behave as a self-consistent set of resistive terms in the MHD equations, thus numerical diffusion cannot be used as a model for Ohmic diffusivity.

Ambipolar diffusion will only be effective when the ionization fraction of the gas becomes so low that ion-neutral collisions are too infrequent to effectively transfer magnetic stresses to the neutral component of the gas. The large ion-neutron drift velocity that may result in this case can serve to redistribute magnetic flux in the gas (Mouschovias 1987), but cannot lead to destruction of flux as in the case of Ohmic diffusivity. We expect ambipolar diffusion to become important only in the outer regions of accretion disks where the temperature and ionization fraction can fall to very low values. Incorporating the effects of ambipolar diffusion into the present model requires the simulation of the full two-fluid MHD equations, which is beyond the scope of this analysis. However, ambipolar diffusion may have significant effects on our results since, in certain regions, it can increase the magnetic braking time (Mouschovias 1987), or if the ion-neutral collision time is longer than the orbital time it can modify the growth of magnetic instabilities (Blaes & Balbus 1993).

4.2. *Nonadiabaticity*

Since the dense cores of protostellar disks are optically thick, we expect their internal dynamics to be adiabatic. However, near the surface of the disk the wind is optically thin and therefore may undergo radiative cooling. Moreover, near the central protostar the strong radiation field from a boundary layer can produce significant heating of the optically thick disk. Modeling the structure of MHD accretion disks near the boundary layer will require detailed radiation hydrodynamic calculations (Stone, Mihalas, & Norman 1992b), such as have been carried out for cataclysmic variable stars (Kley 1989). However, since the energy transport mechanism cannot

directly affect the angular momentum distribution in the disk, nor the magnetic braking or shear instability of the disk (which result from noncompressive magnetic tension forces), nonadiabaticity may have little effect on the evolution observed here.

4.3. *Three-Dimensional Effects*

All of the simulations presented in this paper assume axisymmetry. Fully three-dimensional simulations will be a challenging but vital avenue for future research, as they will allow for a number of important effects. For example, in three dimensions, nonaxisymmetric modes of the Parker instability will be possible. These modes can cause toroidal flux loops to rise buoyantly out of the plane of the disk, thus reducing magnetic pressure gradients which drive the flow. Moreover, as the toroidal field is warped out of the equatorial plane, it can be sheared into a poloidal topology which can couple to the dynamics through magnetocentrifugal effects. Fully three-dimensional simulations will also allow the growth of nonaxisymmetric modes of the BH instability. For example, three-dimensional simulations of the local evolution the instability (Hawley et al. 1994) have shown that the channel solution is unstable to nonaxisymmetric perturbations, thus in three-dimensions it develops into turbulence. Characterizing the nature of this turbulence, and its effect on the global evolution of disks, is an important problem for future studies.

5. CONCLUSIONS

In this paper we have presented time-dependent simulations of the global evolution of magnetic accretion disks. Our primary conclusion is summarized in Figure 1. We have found that axisymmetric disks with purely axial magnetic fields in the initial state always undergo radial collapse on a free-fall timescale. For disks which begin with a Keplerian rotation profile, the collapse is driven either by magnetic braking (for strong magnetic fields) or by magnetic instabilities (for weak magnetic fields). In some cases, we find collapse of the disk at free fall can produce a magnetic-pressure–driven wind. For disks which begin with a sub-Keplerian rotation profile, collapse begins due to the assumed initial conditions.

Although we have performed a large number of simulations (e.g., Stone 1990), in this paper we have discussed only three in detail. Run A began with a sub-Keplerian rotation profile and a strong magnetic field. The centrifugal barrier formed during the essentially hydrodynamic collapse of the disk generates a strong toroidal magnetic field which then drives a highly collimated jetlike outflow along axial magnetic pressure gradients. This simulation reproduces all of the essential features of previous MHD simulations of magnetic accretion disks (US). Run B began with a Keplerian rotation profile and a strong magnetic field ($\beta \lesssim 1$). We found that strong magnetic braking leads to a runaway collapse of the inner portion of the disk on an orbital timescale. Our results indicate the only way such collapse can be avoided is with an extremely large contrast between the densities of the disk and of the corona ($\rho_d/\rho_x \geq 10^3$). Even then, if the disk is stratified, the low-density surface layers can be strongly magnetically braked. Finally, Run C began with a Keplerian rotation profile and a weak magnetic field ($\beta \gtrsim 10$). We find that the disk is unstable to the BH instability. Nonlinear growth of this instability on an orbital timescale leads to a channel solution consisting of high angular momentum material streaming radially outward in the midplane of the disk, and low angular momentum material streaming radially inward at the surfaces of the disk. Such behavior is consistent with previous axisymmetric numerical simulations (Hawley & Balbus 1992) and analytic solutions (Goodman & Xu 1993) to the saturated stage of initially vertical fields. Our results show the distinction between the action of an external torque (magnetic braking) versus an internal torque (BH instability). Moreover, the evolution of the disk and outflow in each we have studied is highly time-dependent, which may indicate that magnetic accretion disks threaded by vertical fields may be intrinsically unsteady.

The simulations presented in this paper are intended as an exploratory study of the global evolution of magnetic accretion disks. A number of important areas for future research are evident, including three-dimensional simulations of the global evolution of BH-unstable disks, the evolution of partially ionized disks (in which the field is only weakly coupled to the fluid), and investigations of the star-disk interface and boundary layer.

We thank Steve Balbus and John Hawley for simulating discussions. The simulations were performed at the National Center for Supercomputing Applications at the University of Illinois. J. M. S. thanks Dimitri Mihalas and the NCSA for suport while much of this work was completed.

REFERENCES

Balbus, S., & Hawley, J. F. 1991, ApJ, 376, 214
———. 1992, ApJ, 400, 610
Blaes, O. M., & Balbus, S. A. 1993, preprint
Blandford, R. D. 1989, in Theory of Accretion Disks, ed. F. Meyer et al. (Dordrecht: Kluwer), 35
Blandford, R. D., & Payne, D. G. 1982, MNRAS, 199, 883
Goodman, J., & Xu, G. 1993, preprint
Hartmann, L., & Kenyon, S. J. 1985, ApJ, 299, 462
Hawley, J. F. 1986, in Radiation Hydrodynamics in Stars and Compact Objects, ed. D. Mihalas & K.-H. Winkler (Berlin: Springer), 369
Hawley, J. F., & Smarr, L. L. 1986, in Magnetospheric Phenomena in Astrophysics, ed. R. Epstein & W. Feldman (AIP Conf. Proc. 144), 263
Hawley, J. F., & Balbus, S. 1991, ApJ, 376, 223
———. 1992, ApJ, 400, 595
Hawley, J. F., Gammie, C. F., & Balbus, S. A. 1994, preprint
Heyvaerts, J., & Norman, C. A. 1989, ApJ, 347, 435
Kley, W. 1989, A&A, 222, 141
Königl, A. 1989, ApJ, 342, 208
Lada, C. J. 1985, ARA&A, 23, 267
Lovelace, R. V. E., Wang, J. C. L., & Sulkanen, M. E. 1987, ApJ, 315, 504
Low, B. C. 1990, ARA&A, 28, 491
Michel, F. C. 1969, ApJ, 158, 727
Mouschovias, T. Ch. 1987, in Physical Processes in Interstellar Clouds, ed. G. Morfill & M. Scholer (Dordrecht: Reidel), 453
Mouschovias, T. Ch., & Paleologou, E. V. 1980, ApJ, 237, 877
Norman, M. L., Clarke, D. A., & Stone, J. M. 1991, Comput. Phys., 3/4, 138
Pelletier, G., & Pudritz, R. E. 1989, ApJ, 394, 117
Sakurai, T. 1987, PASJ, 39, 821
Shibata, K., & Uchida, Y. 1986, PASJ, 38, 631
Shu, F. H., Lizano, S., Ruden, S. P., & Najita, J. 1988, ApJ, 328, L19
Stone, J. M. 1990, Ph.D. thesis, Univ. Illinois
Stone, J. M., Hawley, J. F., Evans, C. E., & Norman, M. L. 1992a, ApJ, 388, 415
Stone, J. M., Mihalas, D., & Norman, M. L. 1992b, ApJS, 80, 819
Stone, J. M., & Norman, M. L. 1992a, ApJS, 80, 753
———. 1992b, ApJS, 80, 791
Uchida, Y., & Shibata, K. 1985, PASJ, 37, 515
Wardle, M., & Königl, A. 1993, ApJ, 410, 218